ADVANCED MATERIALS INTERFACES

www.advmatinterfaces.de

Superhydrophobic Surfaces Based on Fractal and Hierarchical Microstructures Using Two-Photon Polymerization: Toward Flexible Superhydrophobic Films

*Yang Lin, Ran Zhou, and Jie Xu**

Introduction of hierarchical microstructures nowadays is considered as an important method to create superhydrophobic surfaces, but the majority of current studies mainly focus on arbitrary or simple 3D geometries. Therefore, only statistic results or particular conclusions can be obtained. Given this concern, two-photon polymerization (TPP) is applied to create well-defined 3D microstructures with high resolution, including fractal Sierpinski tetrahedrons, and hierarchical pyramid structures. Surfaces that have fractal structures with higher complexity are found to be more hydrophobic than their lower-stage counterparts. Additionally, fractal Sierpinski tetrahedron structures prove to possess higher efficiency in achieving superhydrophobicity when compared to hierarchical pyramids. Further, TPP is also adopted in creating microstructures on flexible substrates. As a demonstration, an array of hierarchical pyramids is fabricated on a plastic film, and superhydrophobicity still remains even after 100 times of bending and relaxing. Moreover, owing to the convenience of spatial control from TPP, tuning of wetting performance in different regions of surfaces is achievable. With this technique, the role of the fractal and hierarchical microstructures in flexible natural creatures can be better understood, thus facilitating the applications, for which robust wetting control is required.

1. Introduction

Nature has long inspired numerous scientific findings and technological innovations, especially after biomimicry was found to be an important approach to tackle human challenges.[1] In particular, living systems such as lotus leaves,[2] insect wings,[3] and rice leaves[4] are usually highly hydrophobic, giving rise to water-repellency, self-cleaning, anti-fouling, and anti-fog, and other appealing properties.[5] Unsurprisingly, these advantages have facilitated the development of artificial hydrophobic materials with a variety of applications coming after, including self-cleaning windows,[6] non-soiling clothing,[7] and wettability treatments on microfluidic devices.[8] Specially, surfaces with extremely high water contact angles and low sliding angles, usually greater than 150° and smaller than 10°, respectively, are considered as superhydrophobic surfaces.[9] It is worth noting that superhydrophobic properties are governed by both surface chemical composition (e.g., surface free energy) and geometrical microstructures (e.g., surface roughness) on the surfaces.[9,10] Therefore, current studies that aim at realizing superhydrophobicity mainly focus on either modifying the chemical properties of the materials or creating efficient microstructures.

Specifically, the impact of geometrical microstructures on surface wetting is attributed to two mechanisms: homogeneous wetting and heterogeneous wetting (**Figure 1**).[11] The former mechanism is also well-known as the Wenzel state, in which the liquid penetrates into the gaps between microstructures, while the latter mechanism is denoted as the Cassie–Baxter state, in which the liquid is supported by the trapped air inside microstructures. Additionally, transition states exist when the tips of the microstructures and substrates show different degrees of heterogeneity.[12] These states result from hierarchical structures, which combine the microscale and nanoscale features. Besides, they have been found in many natural superhydrophobic creations, and proven to be a useful approach to enhance superhydrophobicity,[13] thus arousing great attentions over the past years.

At present, a number of fabrication techniques have been investigated and utilized to create hierarchical structures, including chemical etching,[14] deep reactive-ion etching (DRIE),[15] replica molding,[16] deposition,[17] photolithography,[18] self-assembly,[19] hydrothermal synthesis,[20] electron-beam lithography,[21] soft lithography,[22] laser-assisted etching,[23] direct laser writing,[24] and so forth. However, even though these techniques have successfully produced superhydrophobic surfaces, most of them can only fabricate arbitrary features with random secondary structures or simple

Y. Lin, Prof. J. Xu
Mechanical and Industrial Engineering
University of Illinois at Chicago
Chicago, IL 60607, USA
E-mail: jiexu@uic.edu
Prof. R. Zhou
Mechanical and Civil Engineering
Purdue University Northwest
Hammond, IN 46323, USA
The ORCID identification number(s) for the author(s) of this article can be found under https://doi.org/10.1002/admi.201801126.

DOI: 10.1002/admi.201801126

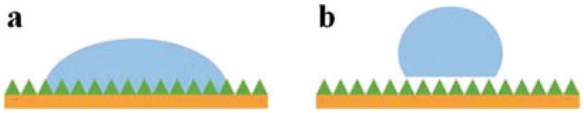

Figure 1. Schematic illustration of two different mechanisms for surface wetting. a) Wenzel state. b) Cassie–Baxter state.

3D structures with extruded shapes.[21] Despite several reports showing that complex 3D shapes can be achieved, their processes are usually quite sophisticated and time-consuming.[25] For instance, dual structure with controllable sidewall profile has been successfully created on a silicon wafer using DRIE combined with black silicon effect.[25a] Further, these methods still lack the ability to create real 3D structures with well-defined geometries, thereby the majority of current studies only reflect either statistic results or particular conclusions drawn based on simple 3D structures. Additionally, current studies mainly focus on creating microstructures on rigid substrates, which lack the softness and flexibility that are ubiquitous in nature. Herein, a simple and accurate way to fabricate controllable 3D microstructures on flexible substrates is still highly demanding for in-depth studying of fundamental principles behind surface wetting as well as creating novel engineering and bionic applications.

Along with the development of additive manufacturing, two-photon polymerization (TPP) has become a promising method to create real 3D microstructures in microscale or submicroscale.[26] During a typical TPP process, a small region (i.e., voxel) in the photosensitive materials is polymerized when two photons are absorbed simultaneously,[27] and final structures fabricated are composed of countless voxels that correspond to the digital files after slicing and hatching (**Figure 2**). Owing to the fact that the resolution of TPP can be as high as 100 nm,[28] various applications such as creating 3D hierarchical structures on the substrates have been realized over past few years. Besides, fractal structures that possess self-similarity on any length scale have also received much attentions for creating superhydrophobicity.[29] Recently, such intrinsically hierarchical structures have been successfully fabricated using TPP as well for wetting study.[30] Furthermore, conventional methods usually consider the whole surface as an entirety, no particular consideration is taken to convert the wetting performance in different areas on the surface. Nevertheless, owing to the intrinsic convenience from additive manufacturing, spatial control can be incorporated into a digital file, thus creating different microstructures to tune wetting performance at different locations. In addition, albeit rigid materials such as silicon and silica are the most commonly used substrates for TPP process, flexible materials possess several unique advantages when creating superhydrophobic films.[31] Compared to their rigid counterparts, flexible materials such as plastics are usually cost-effective, soft, flexible, light, thin, and unbreakable. Additionally, natural superhydrophobic materials are usually of good flexibility, whose effect on the wetting performance has long been ignored. It is only recently found that substrate flexibility enhances superhydrophobic performance along with surface microstructures synergistically.[32] For instance, extended water repellency can be attributed to substrate flexibility, and other droplet effects such as impalement resistance and droplet-substrate contact time also benefit from flexible feature. Last but not least, flexible films can also be used for further bionic studies such as raindrop bouncing on hydrophobic insect wings.

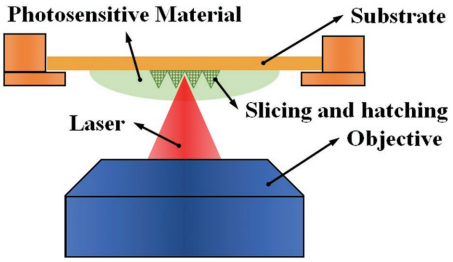

Figure 2. Schematic illustration of a typical TPP fabrication configuration. The final structures are composed of voxels in a typical TPP fabrication process based on slicing and hatching approach.

In this article, we have first adopted TPP technique to fabricate various 3D hierarchical structures on glass slides, including fractal tetrahedron and pyramids arrays, to investigate the impact of 3D hierarchical structures on superhydrophobic behavior. Afterward, hexamethyldisiloxane (HMDSO) was coated on all surfaces via plasma enhanced chemical vapor deposition (PECVD) to further enhance hydrophobicity. Finally, superhydrophobic flexible film was achieved via fabricating hierarchical structures on a plastic film using TPP technique, followed by HMDSO coating. We believe this method could help people to better understand the meaning of fractal and hierarchical structures in nature, and inspire the bionic inventions on flexible substrates for various applications such as biology, chemistry, and microfluidics.

2. Design and Fabrication of Microstructures

2.1. Fractal Microstructures

Apart from regular hierarchical structures that add nanoscale features to microscale backbones, Shibuichi et al. have reported that hierarchical structures with fractality also have the capability in achieving superhydrophobicity.[29] However, previous studies mainly focus on forming random fractal structures on substrates,[9,33] by which the conclusions drawn were statistic. Recently, Davis et al. have designed three fractal structures with different fractal dimensions using TPP,[30] and they found that there was no clear correlation between surface wetting performance and fractal dimensions. This finding deviated from the theory proposed by Shibuichi. Hereby, we have adopted the famous fractal structure (i.e., Sierpinski tetrahedron) to further study the relationship between fractality and surface wetting.

Three stages (0, 1, and 2) of Sierpinski tetrahedron have been adopted in this article. As shown in **Figure 3**a–c, the stage-0 Sierpinski tetrahedron is basically a single tetrahedron without any modification, while the stage-1 Sierpinski tetrahedron consists of four identical stage-0 Sierpinski tetrahedrons with half size. Similarly, stage-2 Sierpinski tetrahedron is composed of four stage-1 Sierpinski tetrahedrons with half size. Herein, four copies of the former stage Sierpinski tetrahedron are connected to each other with corner touching. It is also worth noting that although the volume decreases (approaching zero) as the iteration goes on, the total surface area remains constant.

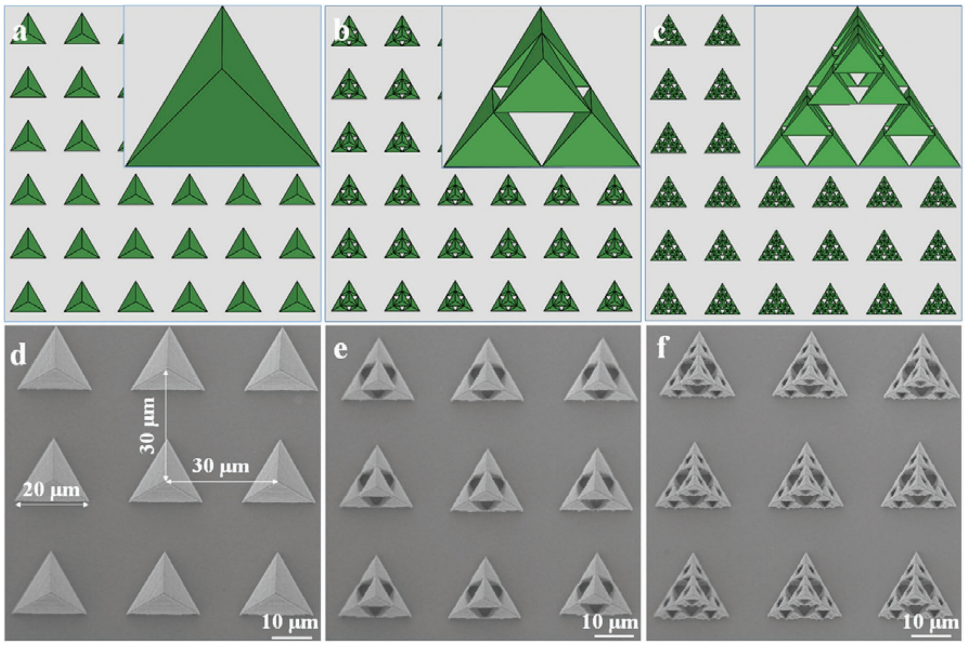

Figure 3. Computer aided design (CAD) models of Sierpinski tetrahedron and corresponding SEM images of the microstructure array fabricated by TPP. a–c) CAD models of stage-0, stage-1, and stage-2 Sierpinski tetrahedron, respectively. d–f) SEM images of stage-0, stage-1, and stage-2 Sierpinski tetrahedron array. The length for each Sierpinski tetrahedron unit is 20 μm and the center-to-center distance between units is 30 μm. The printed surface area is roughly 3 × 3 mm.

In fractal geometry, fractal dimension has been widely used to represent the statistical index of the complexity for objects with self-similarity, and it can be simply calculated using Equation (1),[34]

$$D = -\frac{\log N}{\log \varepsilon} \tag{1}$$

where D is the fractal dimension, N is the number of the parts that form fractal objects, and ε stands for the scaling factor. Hereby, we can simply obtain the fractal dimension of Sierpinski tetrahedron: $D_s = -\log(4)/\log(0.5) = 2$.

As the ratio between height and bottom area is constant, it is obviously pointless to create a single big Sierpinski tetrahedron on a glass substrate, not to mention endless time required for fabrication. Given this concern, we have introduced the array of Sierpinski tetrahedron, in which each unit has a length of 20 μm and a center-to-center distance of 30 μm (Figure 3d–f). Although when taking the whole array into account, it cannot be considered as a fractal object, but fractality still exists in each unit. Moreover, as the microstructures are polymerized voxel by voxel, the required fabrication time increases drastically if the slicing and hatching distances decrease. Therefore, an appropriate selection of printing parameters is indispensable. Hereby, despite finer slicing and hatching (e.g., 0.2 and 0.1 μm, respectively) enable a better result with smoother surface finishing, the time cost can be tens of that for normal slicing and hatching (e.g., 0.4 and 0.3 μm used in this article, respectively). However, if they are further increased, the overlaps at corners where tetrahedrons touch become insufficient, thus the top structures may be washed away during development of photosensitive materials. Furthermore, the surface finishing may become unfavorable, even leading to severe deformation.

2.2. Conventional Hierarchical Microstructures

In addition to the fractal Sierpinski tetrahedron described above, conventional hierarchical structures with real 3D shapes were also fabricated on glass substrates. Three patterns of microstructure composed of rectangular pyramids have been utilized. The first pattern is an array that consists of single pyramids (**Figure 4**a), with the length of the square base and height of 20 μm. On the contrary, the second pattern is composed of hierarchical pyramids that contain smaller pyramids (Figure 4b). In spite of the sizes of square base and height being identical to the first pattern, their main bodies are filled with 36 small pyramids with length and height of 2.5 μm. Furthermore, we also created the third pattern, in which the entire printing area was covered with hierarchical pyramids as well as the small pyramids in between (Figure 4c). In order to maintain the height of microstructures, the angles of the pyramids in the second and the third patterns were different to that of the first one. It is also worth mentioning that clear ridges were found under scanning electron microscope (SEM) (Figure 4d–f), and this discrepancy can be alleviated by decreasing the values of slicing and hatching.

2.3. Measurement and Analysis of Surface Wettability

After TPP fabrication, we measured the contact angles for all the surfaces with different microstructures described above. Here, we used indium tin oxide (ITO)-coated glass slides as the substrates. The coated ITO allowed the TPP system to find the interface between the glass slides and dropped photosensitive materials. A bare substrate without any printed structure and a

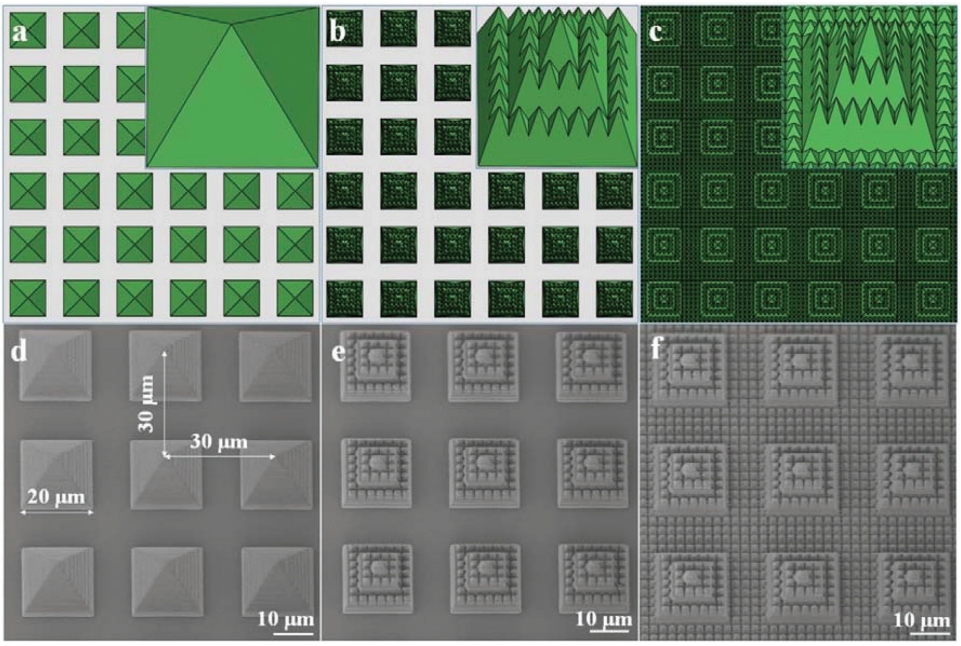

Figure 4. CAD models of the hierarchical pyramids and corresponding SEM images of the microstructure array fabricated by TPP. The tilt angle used for SEM is 15°. a) CAD model of the array of rectangular pyramids, which has a length of 20 μm for square base and height of 20 μm. b) CAD model of the array of hierarchical pyramids, in which the main bodies are filled with 36 smaller rectangular pyramids with length and height of 2.5 μm. c) CAD model of the microstructures by which the entire printing area is covered with hierarchical and small pyramids. d) SEM image of the array with pyramids. e) SEM image of the array with hierarchical pyramids. f) SEM image of the array with entirely hierarchical structures.

substrate with a flat square structure (length of 3 mm and thickness of 10 μm) were used as controls. As shown in **Figure 5**a, although the array of fractal Sierpinski tetrahedron structures improved the hydrophobicity of the surfaces when the complexity increased, their wetting performances were still not great. This was attributed to the photosensitive resist (i.e., IP-S) used for TPP, as it displayed a slightly hydrophilic behavior, which has been proved using a flat structure as control. Thereby the wetting was at Wenzel state. Moreover, albeit the surface with array of stage-2 Sierpinski tetrahedron structures displayed a hydrophobic behavior, contact angle decreased abruptly within 1 min, manifesting that the wetting state transferred from

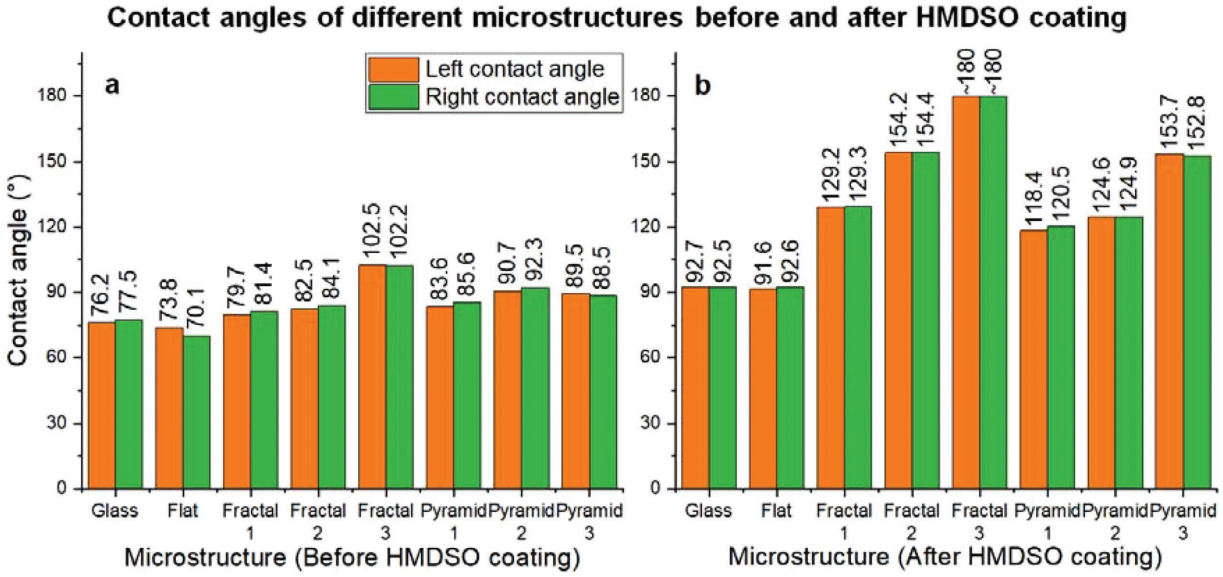

Figure 5. Left and right contact angles of the surfaces with different microstructures before and after HMDSO coating. a) All the contact angle measurements were conducted before HMDSO coating. b) All the contact angle measurements were conducted after HMDSO coating. The samples in both bar charts from left to right are bare ITO-coated glass, glasses with flat IP-S structure, stage-0 Sierpinski tetrahedron array, stage-1 Sierpinski tetrahedron array, stage-2 Sierpinski tetrahedron array, rectangular pyramid array, hierarchical pyramid array, and entirely hierarchical pyramid array, respectively.

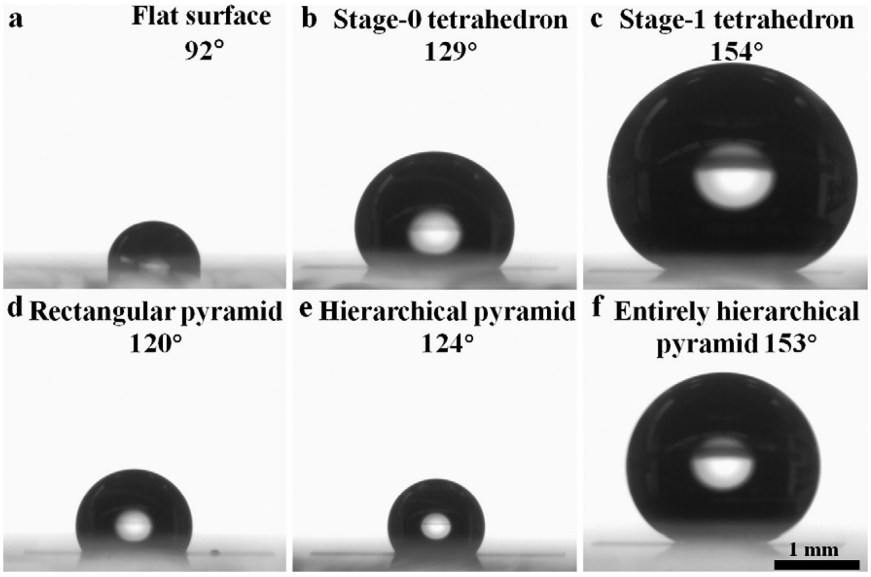

Figure 6. Images of the sessile drops sat on surfaces with various structures: a) Flat structure; b) Array of stage-0 Sierpinski tetrahedrons; c) Array of stage-1Sierpinski tetrahedrons; d) Array of rectangular pyramids; e) Array of hierarchical pyramids; f) Structure of entirely hierarchical pyramids.

Cassie state to Wenzel state. Additionally, the array of hierarchical pyramids only exhibited a slight hydrophobicity when compared to the original array of rectangular pyramids, while the entirely hierarchical pyramid structure even displayed a hydrophilic behavior.

In order to reduce the surface energy for these surfaces, a thin (C:H:Si:O) film (≈ 100 nm) was deposited on all samples using HMDSO via PECVD.[13] Herein, the negative impact from photoresist was alleviated as shown in Figure 5b. It is worth noting that the flat surface fabricated via TPP possessed a relatively smaller contact angle compared to that of a bare ITO-coated glass slide. However, the other surfaces had exhibited a much more hydrophobic behavior. For example, surface with the array of stage-0 Sierpinski tetrahedrons exhibited a static contact angle of 129°, and surface with the array of stage-1 Sierpinski tetrahedrons displayed superhydrophobicity as its contact angle was larger than 150°. Furthermore, we failed to measure precisely the contact angle from surface of stage-2 Sierpinski tetrahedron as the water droplets merely rolled on the surface rather than forming a sessile drop. This phenomenon manifested that the surface possessed even better superhydrophobicity, indicating a contact angle close to 180°. Additionally, it is worth noting that the sizes of the sessile water droplets for each design were different due to the fact that small droplets were difficult to introduce to the surface when the hydrophobicity increased. Herein, big droplets were adopted for more hydrophobic surfaces. Although the difference of Laplace pressure varied if the size of sessile drop changed, the results shown in **Figure 6** were sufficient to indicate that fractal structure was more efficient than hierarchical pyramid in terms of imparting hydrophobicity to the surfaces especially when considering that the fabrication time of fractal structures were significantly less (60–70% reduction).

Despite the fact that all the fractal structures had the same fractal dimension of 2, their hydrophobicity increased when the complexity increased, which was similar to the performance of untreated counterparts. This can be attributed to the fact that small openings between components from these fractal structures inhibited the penetration of the water, thus maintaining the Cassie state. Moreover, this phenomenon also implied that fractal dimension is not the only or main factor that governs the wetting performance for fractal microstructures. Besides, compared to the untreated surfaces, the contact angle remained almost constant for more than 20 min. Even though continuous evaporation of water increased the Laplace pressure of the droplet (due to decreasing radius of curvature), there was no abrupt change of contact angle occurred. This indicated that the microstructures had maintained the Cassie state.

On the other hand, array of hierarchical pyramid was also proven to be efficient for obtaining superhydrophobic surfaces. However, it is worth mentioning that only the entirely hierarchical structure possessed the contact angle more than 150°, associated with a slicing angle of 2°. Herein, it was not as efficient as fractal structures for creating superhydrophobic surfaces in terms of fabrication time. Moreover, as there was no free space in the entirely hierarchical structure, this design is not favorable for flexible films.

2.4. Flexible Hydrophobic Surfaces

As aforementioned, flexibility is ubiquitous in natural superhydrophobic creations, and it has been proven to be beneficial for the performance of surface wetting. Herein, besides creating microstructures on glass slides as described above, we have also investigated the wetting properties of 3D microstructures on a flexible substrate. Polyethylene terephthalate (PET) is one of the most commonly used polyesters nowadays due to its attractive properties such as high tensile strength and transparency as well as favorable chemical, mechanical, and thermal stability.[35] Recently, PET films have aroused increasing attentions in various applications such as flexible electronics,[36] flexible microfluidics,[37] and advanced sensors.[38] Herein, ITO-coated PET film was chosen as a demonstration for surface wetting study. During the fabrication process, a glass slide was attached to the PET film as a mechanical support to prevent film deformation. Besides, an array of hierarchical pyramids was used as a concept-proofing example (**Figure 7**a), followed by HMDSO coating. Since hierarchical microstructures in the array were disconnected from each other, detachment of the microstructures did not happen after 100 cycles of bending and relaxing, giving rise to a robust flexible hydrophobic film. In addition, the fabricated surface has indicated the performance of superhydrophobicity (**Table 1**), and its left, right contact angles, and slicing angle were

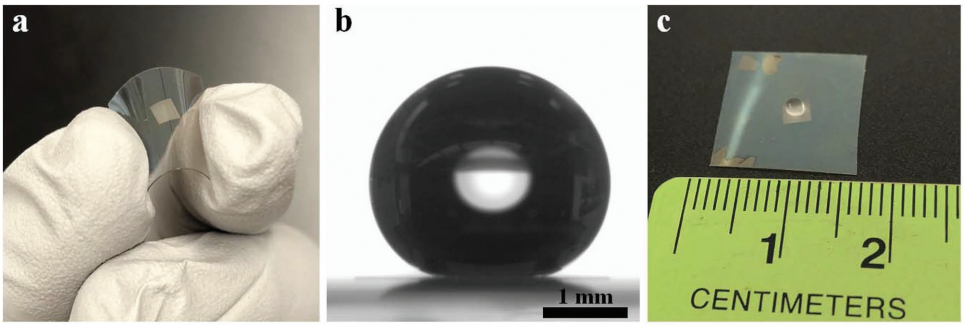

Figure 7. Flexible superhydrophobic film achieved by creating microstructures on a PET film using TPP technology. a) Photo of the as-prepared superhydrophobic PET film. b) Image that showed the behavior of superhydrophobicity of PET film with hierarchical microstructures. c) Photo of the sessile drop of water on a PET film. Photos were taken using an iPhone 8.

measured to be 156.5°, 157.8°, and 2°, respectively (Figure 7b,c), which was larger than that of the same structure on glass slides.

3. Conclusion

In this article, various 3D hierarchical structures have been created on glass slides and flexible PET films using TPP technique, including fractal Sierpinski tetrahedron and hierarchical pyramid microstructures. We found that untreated microstructures only slightly increased the hydrophobicity of the surfaces, and this can be attributed to the intrinsic hydrophilicity of the photoresist IP-S. Nevertheless, after depositing a thin layer of HMDSO onto the surfaces, the microstructures have proven to be useful for imparting hydrophobicity. It was worth noting that although all three stages of Sierpinski tetrahedron have the same fractal dimension of 2, better hydrophobicity was obtained when the complexity increased. Stage-1 and stage-2 Sierpinski tetrahedron have proven their ability in creating superhydrophobic surfaces. On the other hand, superhydrophobicity can also be achieved when applying hierarchical pyramids to the surfaces. However, only the microstructures that covered the printing area completely with pyramids had this ability, making the method inefficient when compared to fractal structures as more fabrication time was required. Moreover, a PET film was also adopted as a demonstration for printing microstructures on flexible substrates using TPP technique. The PET film with microstructures maintained good hydrophobicity after bending and relaxing for more than 100 times. Herein, this method is simple and offers several advantages compared to existing methods. To name a few, it does not require complex operations such as wet etching to obtain 3D structures. Complex structures like Sierpinski tetrahedron are no longer unachievable. Digital files used in TPP are easier to change than other fabrication protocols, hereby promoting prototyping developments. Besides, TPP technique allows the creation of different microstructures at different regions on a surface, making the surface wetting controllable. Lastly, this approach can also be applied in flexible materials that are cheaper, robust, and provide a better similarity to natural creations, by which studies on surface wetting and other phenomena in nature can be further investigated. Nevertheless, there is one downside of using TPP technique, namely, the fabrication speed. Owing to its intrinsic voxel-by-voxel fabrication mechanism, the process of TPP nowadays is still not fast enough to achieve mass production. However, various approaches have been proposed to make TPP process faster. To name a few, novel photoinitiators that possess wide dynamic range have been proven to enable a faster TPP process.[39] Moreover, when considering the fabrication of a pattern using TPP, multiple static or dynamic beams are also good choices.[40] For example, multiple focal points (up to hundreds) can be obtained using a microlens array, giving rise to simultaneous polymerization in different areas.[41] Thereby, the fabrication time for creating superhydrophobic surfaces using microstructure patterns can be reduced drastically, and large surfaces can also be realized. In addition, an optimal balance of laser intensities, chemical reaction rates as well as the movements of galvo mirrors and stages also leads to a much faster fabrication speed. To conclude, we believe the proposed method has opened a new door for further study of surface wetting with respect to the performance of real 3D microstructures on flexible substrates, and it can also be a useful tool for the development of surface engineering and other important fields such as biology, chemistry, flexible electronics, and microfluidics.

Table 1. Left and right contact angles of flexible PET films before and after HMDSO coating.

Structure	θ_{left}	θ_{right}	θ_{left} (HMDSO)	θ_{right} (HMDSO)
Bare ITO-coated PET film	77.5°	76.7°	90.1°	90.1°
PET film with hierarchical pyramids	95.3°	93.2°	156.5°	157.8°

4. Experimental Section

Materials and Equipment: ITO-coated square glasses (length: 25 mm, thickness: 0.7 mm) and IP-S photoresist were purchased from Nanoscribe GmbH. ITO-coated PET film (thickness: 0.127 mm) was purchased from Sigma-Aldrich. Propylene glycol monomethyl ether acetate (PGMEA) was purchased from MicroChem. Photonic Professional System from Nanoscribe GmbH was used to create microstructures on either glass or PET substrates. Polaron E5100 Series II sputter coater was used for gold deposition. JEOL JSM-6320F field emission scanning electron microscope (FESEM) was used for SEM imaging. Low-pressure plasma system Tetra 100 PC / PCCE was

used for HMDSO deposition with the help of Diener Electronic GmbH. DataPhysics OCA 25 was used to measure the contact angle.

TPP Fabrication on Glass Substrates: ITO-coated glasses were first thoroughly cleaned with acetone and isopropyl alcohol (IPA), followed by blow-drying with nitrogen. Afterward, they were mounted on the holder with tape, and a small drop of IP-S photoresist was carefully added onto the surface of substrates. Then the holder was loaded into Nanoscribe system, and 25× 0.8NA objective was selected for fabrication. Although 63 × 1.4NA objective enables a better resolution and surface finishing, associated fabrication time would increase drastically. Slicing distance of 0.4 µm and hatching distance of 0.3 µm were adopted when creating the job files using DeScribe software. Moreover, as the pattern fabricated was roughly 3 mm × 3 mm, stitching was inevitable due to the limitation from each printing field, as it was only around 270 × 270 µm. Therefore, an array of 11 × 11 patterns was adopted during fabrication process, and the fabrication time varied from 1.5 to 3.5 h for different designs (entirely hierarchical microstructures required much more time: 10 h). After the fabrication finished, the samples were developed using PGMEA for 10 min, followed by IPA rinse and air drying.

TPP Fabrication on PET Films: Basically, the fabrication of microstructures on PET films is quite similar to that for glass substrates. However, as the PET film was flexible and much thinner than glass, a square glass (length of 25 mm and thickness of 0.7 mm) was adopted as a support. Specifically, the glass was first placed on the holder, then cleaned PET film was cut into appropriate size (e.g., 2 × 2 mm), followed by mounting together with tape. It was also worth noting that Nanoscribe system capitalized on the differences of refractive indices between substrates and photoresist to find interfaces, thereby the interface between PET film and glass support may interfere with correct interface. Given this concern, a small droplet of IPA was added on the glass before mounting the PET film, thus the trapped IPA film masked the interference from another interface.

SEM Imaging: A 10 nm layer of gold was deposited on the samples before SEM imaging. Afterward, the samples were transferred to JEOL JSM-6320F FESEM, and an acceleration voltage of 3.0 kV was applied for imaging.

HMDSO Treatment: HMDSO treatment was conducted with the help of Diener Electronic GmbH. Basically, the samples were activated with oxygen plasma first, then PECVD was used to coat a 100 nm layer of HMDSO.

Contact Angle Measurement: Contact angle was measured using a DataPhysics OCA 25 goniometer. Deionized (DI) water droplets were carefully added onto the surfaces of samples and their sizes varied depending on wetting behaviors. Afterward, images and contact angles were recorded and measured using SCA20 software. All the measurements were conducted under the temperature of 22 °C and humidity of 45%.

Acknowledgements

This work was supported by an Early Career Faculty grant (80NSSC17K0522) from NASA's Space Technology Research Grants Program. The authors appreciate the assistance provided by Dr. Sushant Anand and Hassan Bararnia in helping with contact angle measurement.

Conflict of Interest

The authors declare no conflict of interest.

Keywords

flexible substrate, fractal structures, hierarchical structures, superhydrophobic surfaces, two-photon polymerization

Received: July 23, 2018
Revised: August 22, 2018
Published online:

[1] J. M. Benyus, *Biomimicry: Innovation Inspired by Nature*, Morrow, New York **1997**.
[2] Y.-T. Cheng, D. E. Rodak, *Appl. Phys. Lett.* **2005**, *86*, 144101.
[3] D. Byun, J. Hong, J. H. Ko, Y. J. Lee, H. C. Park, B.-K. Byun, J. R. Lukes, *J. Bionic Eng.* **2009**, *6*, 63.
[4] L. Feng, S. Li, Y. Li, H. Li, L. Zhang, J. Zhai, Y. Song, B. Liu, L. Jiang, D. Zhu, *Adv. Mater.* **2002**, *14*, 1857.
[5] B. Liu, Y. He, Y. Fan, X. Wang, *Macromol. Rapid Commun.* **2006**, *27*, 1859.
[6] C. Yang, U. Tartaglino, B. Persson, *Phys. Rev. Lett.* **2006**, *97*, 116103.
[7] K. Ramaratnam, V. Tsyalkovsky, V. Klep, I. Luzinov, *Chem. Commun.* **2007**, *43*, 4510.
[8] T. Sun, L. Feng, X. Gao, L. Jiang, *Acc. Chem. Res.* **2005**, *38*, 644.
[9] A. Synytska, L. Ionov, K. Grundke, M. Stamm, *Langmuir* **2009**, *25*, 3132.
[10] J. Wu, J. Xia, W. Lei, B. Wang, *PLoS One* **2010**, *5*, e14475.
[11] V. Hejazi, A. D. Moghadam, P. Rohatgi, M. Nosonovsky, *Langmuir* **2014**, *30*, 9423.
[12] M. Berwind, A. Hashibon, A. Fromm, M. Gurr, F. Burmeister, C. Eberl, *Microfluid. Nanofluid.* **2017**, *21*, 144.
[13] T.-G. Cha, J. W. Yi, M.-W. Moon, K.-R. Lee, H.-Y. Kim, *Langmuir* **2010**, *26*, 8319.
[14] Y. Xiu, Y. Liu, D. W. Hess, C. Wong, *Nanotechnology* **2010**, *21*, 155705.
[15] Y. Kwon, N. Patankar, J. Choi, J. Lee, *Langmuir* **2009**, *25*, 6129.
[16] S. J. Choi, S. Y. Huh, *Macromol. Rapid Commun.* **2010**, *31*, 539.
[17] H. Wu, D. Lin, W. Pan, *Langmuir* **2010**, *26*, 6865.
[18] L. F. Boesel, C. Greiner, E. Arzt, A. Del Campo, *Adv. Mater.* **2010**, *22*, 2125.
[19] B. Pokroy, S. H. Kang, L. Mahadevan, J. Aizenberg, *Science* **2009**, *323*, 237.
[20] J. Wu, J. Xia, Y.-n. Zhang, W. Lei, B.-p. Wang, *Phys. E* **2010**, *42*, 1325.
[21] J. Feng, M. T. Tuominen, J. P. Rothstein, *Adv. Funct. Mater.* **2011**, *21*, 3715.
[22] M. D. Morariu, N. E. Voicu, E. Schäffer, Z. Lin, T. P. Russell, U. Steiner, *Nat. Mater.* **2003**, *2*, 48.
[23] T. Baldacchini, J. E. Carey, M. Zhou, E. Mazur, *Langmuir* **2006**, *22*, 4917.
[24] O. Tricinci, T. Terencio, B. Mazzolai, N. M. Pugno, F. Greco, V. Mattoli, *ACS Appl. Mater. Interfaces* **2015**, *7*, 25560.
[25] a) G. Sun, T. Gao, X. Zhao, H. Zhang, *J. Micromech. Microeng.* **2010**, *20*, 075028; b) Y. Liu, A. Das, Z. Lin, I. B. Cooper, A. Rohatgi, C. Wong, *Nano Energy* **2014**, *3*, 127.
[26] Y. Lin, J. Xu, *Adv. Opt. Mater.* **2018**, *6*, 1701359.
[27] Y. Lin, C. Gao, D. Gritsenko, R. Zhou, J. Xu, *Microfluid. Nanofluid.* **2018**, *22*, 97.
[28] A. Ovsianikov, B. N. Chichkov, in *Two-Photon Polymerization – High Resolution 3D Laser Technology and Its Applications* (Eds.: A. Korkin, F. Rosei), Springer, New York **2008**, p. 427.
[29] S. Shibuichi, T. Onda, N. Satoh, K. Tsujii, *J. Phys. Chem.* **1996**, *100*, 19512.
[30] E. Davis, Y. Liu, L. Jiang, Y. Lu, S. Ndao, *Appl. Surf. Sci.* **2017**, *392*, 929.
[31] a) L. Wang, Q. Gong, S. Zhan, L. Jiang, Y. Zheng, *Adv. Mater.* **2016**, *28*, 7729; b) X. Liu, H. Gu, M. Wang, X. Du, B. Gao, A. Elbaz, L. Sun, J. Liao, P. Xiao, Z. Gu, *Adv. Mater.* **2018**, *30*, 1800103; c) H.-J. Kwon, J. Yeo, J. E. Jang, C. P. Grigoropoulos, J.-H. Yoo, *Materials* **2018**, *11*, 1226.
[32] T. Vasileiou, J. Gerber, J. Prautzsch, T. M. Schutzius, D. Poulikakos, *Proc. Natl. Acad. Sci.* **2016**, *113*, 13307.
[33] Y. Xu, D. Wu, Y. H. Sun, Z. X. Huang, X. D. Jiang, X. F. Wei, Z. H. Li, B. Z. Dong, Z. H. Wu, *Appl. Opt.* **2005**, *44*, 527.
[34] C. Faloutsos, V. Gaede, *Computer Science Department* **1996**, 548.
[35] Z. Ke, B. Yongping, *Mater. Lett.* **2005**, *59*, 3348.
[36] V. Zardetto, T. M. Brown, A. Reale, A. Di Carlo, *J. Polym. Sci., Part B: Polym. Phys.* **2011**, *49*, 638.

[37] J. C. Yeo, J. Yu, Z. M. Koh, Z. Wang, C. T. Lim, *Lab Chip* **2016**, *16*, 3244.
[38] C. Pang, C. Lee, K. Y. Suh, *J. Appl. Polym. Sci.* **2013**, *130*, 1429.
[39] Z. Li, N. Pucher, K. Cicha, J. Torgersen, S. C. Ligon, A. Ajami, W. Husinsky, A. Rosspeintner, E. Vauthey, S. Naumov, *Macromolecules* **2013**, *46*, 352.
[40] a) T. Baldacchini, *Three-Dimensional Microfabrication Using Two-Photon Polymerization: Fundamentals, Technology, and Applications*, William Andrew Publishing, Norwich, New York **2015**; b) B. Xu, W.-Q. Du, J.-W. Li, Y.-L. Hu, L. Yang, C.-C. Zhang, G.-Q. Li, Z.-X. Lao, J.-C. Ni, J.-R. Chu, *Sci. Rep.* **2016**, *6*, 19989.
[41] F. Formanek, N. Takeyasu, T. Tanaka, K. Chiyoda, A. Ishikawa, S. Kawata, *Appl. Phys. Lett.* **2006**, *88*, 083110.

